BIS ENERGY AND ENGINEERING

Volume 2 2025 | DOI: 10.31603/biseeng.207
6th Borobudur International Symposium on Science and Technology (BIS-STE) 2024

UNIMMA PRESS
UNIVERSITAS MUHAMMADIYAH MAGELANG

Influence of AA2024-O inserted material on microstructure and mechanical properties of FSWed AA5083-H112 joints

Aszul Kifrun[1], M.N. Ilman[1*]

[1] Department of Mechanical and Industrial Engineering, Universitas Gadjah Mada (UGM), Yogyakarta, Indonesia
[*] Corresponding author email: ilman_noer@ugm.ac.id

Abstract

The present paper is aimed to study microstructure and mechanical properties of friction stir welded (FSWed) AA5083-H112 aluminum alloy butt joints fabricated by inserting AA2024-O aluminum alloy thin foil. In this research, a thin AA2024-O foil with the size of 2 x 3 x 300 mm^3 was inserted between the faying surfaces of two AA5083-H112 plates to be joined. FSW process was conducted using tool rotational speed of 1500 rpm, tool traveling speed of 30 mm/minute, and tool tilt angle of 2^o. After welding, microstructural, hardness, and tensile properties of the FSWed joints without and with inserted AA2024-O thin foil were compared. Results showed that FSWed joints with inserted AA2024-O material have an ultimate tensile strength (UTS) of 249.8 MPa which was higher than that of conventional FSW joints (220.8 MPa). Similarly, the weld nugget zone (WNZ) fabricated using the inserted material has higher hardness compared to that produced by conventional FSW. The improved mechanical properties of the FSW joints having inserted AA2024-O material could be related to the occurrence of diffusion from the inserted material into AA5083-H112 plates combined with precipitation hardening.

Keywords

Friction stir welding (FSW), AA5083-H112 aluminum alloy, Insert material, Microstructure, Mechanical properties

Published:
May 31, 2025

Selection and Peer-review under the responsibility of the 6th BIS-STE 2024 Committee

Introduction

Aluminum alloys such as 5xxx series (Al-Mg) fulfill the requirements for structures and machines since the alloys have high ratio of strength-to-weight, good toughness, weldability and resistance to seawater corrosion [1]. From metallurgical point of view, 5xxx series are non-heat treatable Al-Mg alloys in which their strength is achieved by solid solution and work hardening mechanisms [2,3]. AA5083 aluminum alloy is one of the 5xxx series which is broadly employed in the construction of naval structures, marine machinery, and underwater vehicles. In general, AA5083 and its 5xxx series are weldable using traditional arc welding processes such as metal inert gas (MIG) and tungsten inert gas (TIG). However, these welding processes are high energy welding processes so that some problems may arise such as porosity and coarser microstructure which degrade weld mechanical properties, distortion and residual stress. These problems may be reduced by the use of friction stir welding (FSW) process which join metals without melting.

FSW is a solid-state welding process which was initially introduced by The Welding Institute (TWI), UK in 1991 [4] and the basic principles of FSW process are given elsewhere [5,6,7]. FSW technique has numerous advantages compared to conventional welding techniques, including reduced distortion, diminished hot cracking and porosity, enhanced mechanical properties, and shorter processing times [8]. Numerous studies have validated the superiority of this welding technique. Nonetheless welding of aluminum alloys, especially the 5xxx series using the FSW method faces a serious challenge. This is because the use of FSW process for 5xxx series aluminum alloy can cause a reduction in mechanical properties in the weld nugget zone (WNZ) and heat affected zone (HAZ) [9]. To improve the mechanical properties of FSW joints, several methods have been developed including modifications to welding tool [10,11,12], optimization of process parameters [13,14,15], cold working [16,17] and the incorporation of micro or nano particles into the weld zone to create localized composites [18,19].

Apart from the methods previously mentioned, the mechanical properties of FSW joints can also be increased by introducing alloying elements at the faying surface of the adjoining plates. This technique is done by inserting a material sheet between the contact surfaces during the FSW process. Recently, several alloying elements have been studied to improve the mechanical properties of aluminum alloy FSW joints. Lenin et al. [20] have reported that inserting zinc (Zn) alloy sheet improved both hardness and tensile strength of the FSW joints of AA 7020 with the best result was achieved at the interlayer thickness of 10 μm. Subsequently, Shiri et al. [21] have investigated various insert materials, i.e. pure Cu, pure Zn, Cu-Zn and Cu-Zn-Ni alloys in FSW process of pure Al plates. The results indicated that the diffusion caused solid solution in stir zone resulting in increased tensile strength of the FSW joints. Recently, copper (Cu) and tin (Sn) have been evaluated as insert materials for FSW process of pure Al by Dixit et al [22]. The results revealed that a fine crack formed at the weld inserted using tin material hence decreasing the quality of the FSW joints.

Although research works on insert materials using various alloying elements have been conducted extensively but none of them is reported to use AA2024-O as insert material. Therefore, the present study is aimed to evaluate the heat treatable AA2024-O as insert material for FSW process of AA5083-H112 plates.

Materials and Methods

In this study, an AA2024-O alloy sheet with dimensions of 300 mm long, 3 mm wide and 2 mm thick was used for the alloying elements. This alloying sheet was positioned between the faying surfaces of AA5083-H112 plates having the dimensions of 300 mm x 100 mm x 3 mm. The compositions of these materials are given in detail in Table 1. FSW processes were conducted using the inserted AA2024-O material as shown in Figure 1(a) with the tool dimensions employed are shown Figure 1(b). The tool had a shoulder diameter of 12 mm whereas its pin geometry is machined in the form of a cylindrical pin having the pin diameter of 5 mm and a pin length of 2.8 mm. As the reference, FSW process without the inserted material was also conducted.

Table 1. Chemical compositions of AA5083-H112 plates and the AA2024-O insert material

Material	Si	Fe	Cu	Mn	Mg	Zn	Cr	Ti	Al
AA5083-H112	0.06	0.24	0.015	0.61	4.51	0.008	0.088	0.024	Bal.
AA2024-O	0.49	0.48	4.50	0.64	1.52	0.11	0.05	0.03	Bal.

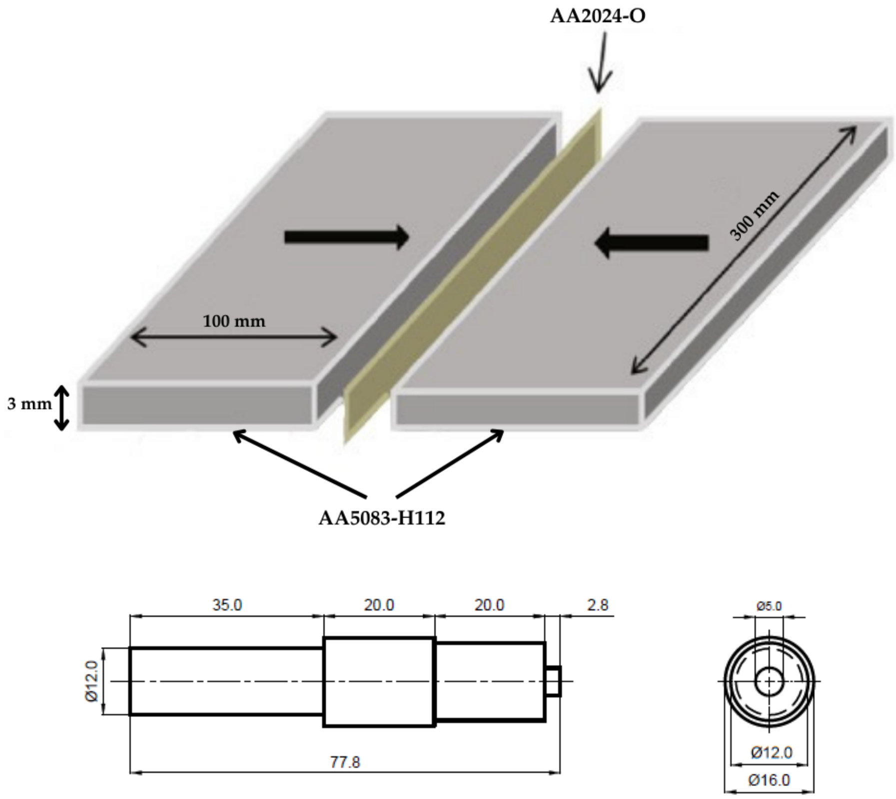

Figure 1. (a) Schematic view of FSW process, (b) Dimensions of tool (mm)

The welding processes were executed using an Aciera knee-type vertical milling machine. The processing parameters used are the followings: (1) tool rotational speed of 1500 rpm, (2) tool traveling speed of 30 mm/min, and (3) tool tilt angle of 2°. After welding, several experiments were conducted including microstructure analysis, a micro-hardness test, and tensile test combined with fractographic study.

Microstructure examinations were carried out using light microscopy and scanning electron microscopy (SEM) combined with energy dispersive X-ray (EDX-ray) analysis. The samples were first cut to get the cross section of FSW joints followed by grinding using emery papers from 150 to 2000 grit, polishing and finally etching using Keller's reagent (25 ml HCl + 25 ml HNO_3 + 2 ml HF + 25 ml H_2O). Subsequently, the Vickers microhardness measurements were conducted across various zones of FSW joints using a test force of 100 g and a dwell time of 10 seconds whereas the distance between two indentation points was 0.5 mm. Finally, tensile tests were performed using a servo-hydraulic universal testing machine with transverse weld specimens were machined following ASTM E8 standard. The tensile parameters measured during the tensile tests were ultimate tensile strength (UTS), yield strength (YS) and ductility given in % elongation. Following the tensile tests, the fracture surfaces of the FSW joints were analyzed using a low magnification optical microscopy and SEM.

Results and Discussion

Macro and Microstructure

Figure 2a illustrates the macrostructure of FSWed AA5083-H112 joint without inserted material with the microstructures obtained from advancing side (AS), weld nugget zone (WNZ) and retreating side (RS) are depicted in Fig. 2(b), (c), (d) respectively. Subsequently, both AS and RS are divided into three regions, namely (1) thermomechanically affected zone (TMAZ), (2) heat affected zone (HAZ), and (3) base metal (BM) as described by Fratini et al. [23]. The FSW profile in Figure 2(a) reveals an unsymmetrically inverted trapezoidal form with the AS is longer than RS. The microstructure of WNZ in Figure 2(c) is characterized by the formation of fine equiaxed grains as the result of dynamic recrystallization during welding. In addition, the WNZ microstructure appears to be homogeneous with some onion rings are observed. The presence of onion rings is likely caused by friction heating resulted from the tool rotation. This rotation causes the forward movement which extrudes the metal surrounding the RS of the tool [24]. The microstructures of TMAZ and HAZ in AS as shown in Figure 2(b) are different to those observed in RS in Figure 2(d) in terms of grain size and grain morphology.

The macrostructure of FSWed AA5083-H112 joints inserted using AA2024-O material are presented in Figure 3a whereas the microstructures in AS, WNZ and RS are depicted in Figure 3(b), (c), (d) respectively. It is seen that the macrostructure in Figure 3(a) reveals the flow direction of the insert material from AS to RS. The dark region in the center of WNZ in Figure 3(a) is rich in AA2024-O whereas the upper surface is mainly AA5083-H112. In the bottom surface, the AA2024-O inserted material is difficult to mix with the AA5083-H112 base metal and under this condition, diffusion may not occur. This observation is based on the response of metal to etchant, i.e. AA2024-O is more susceptible to corrosion than AA5083-H112, therefore AA2024-O appears to be darker. These results will be clarified using SEM equipped with EDX-analysis in the next section.

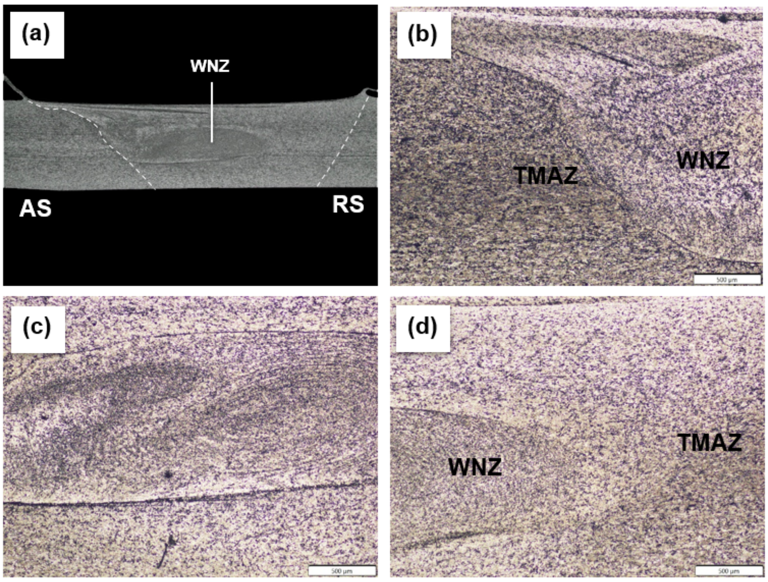

Figure 2. (a) Macrostructure of FSW joint of AA5083-H112 and (b),(c),(d) Microstructure in AS region, WNZ and RS region respectively

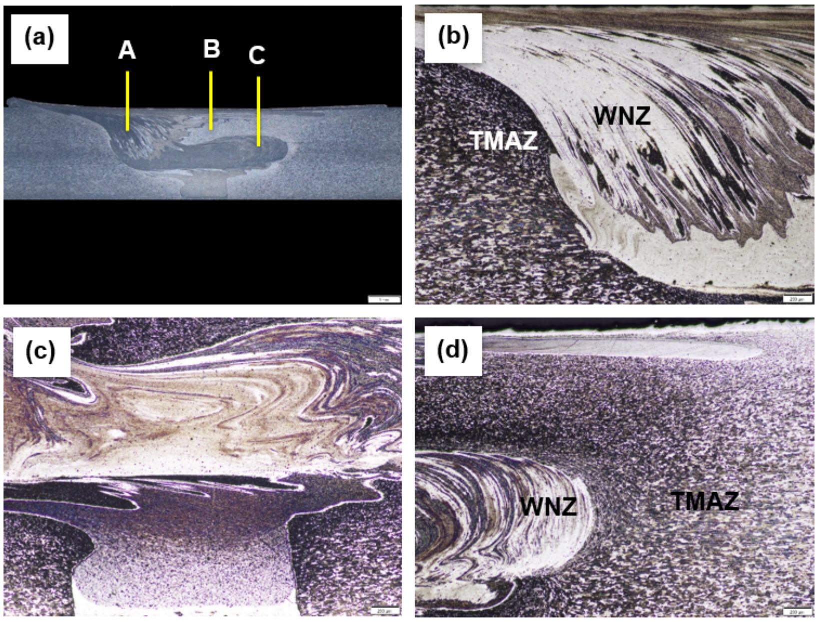

Figure 3. (a) Macrostructure of FSWed AA5083-H112 joint with inserted AA2024-O alloy and b,c,d microstructure in AS region, WNZ and RS region respectively.

Microstructures of TMAZ and HAZ in AS (Figure 3(b)) and RS (Figure 3(d)) show significant differences in terms of grain size and grain morphology. In WNZ in Figure 3(c), various distinct regions are observed due to stirring action by a pin and a shoulder of the tool during FSW process. This appearance suggests that the insert material and the base metal have been already mixed with the diffusion may occur.

Apart from optical microscopy, various different regions in WNZ labeled A, B and C in Figure 3(a) are identified using Energy Dispersive X-ray (EDX) analysis with the results are shown in Figure 4(a), (b), (c). The EDX spectra obtained from the region marked A close to AS in Figure 3(a) are shown in Figure 4(a). The region A is composed of mainly

Cu around 15.5 wt.% with a low content of Mg, typically 1.02 wt.%. This Cu rich region is formed due to the mass flow of AA2024-O from AS towards the weld center. Region B reveals the spectra containing 4.05 wt.% Mg without any Cu content suggesting that this region is pure AA5083-H112 as depicted in Figure 4(b). Finally, as can be seen in Figure 4(c), region C consists of 3.23 wt.% Mg and 1.36 wt.% Cu suggesting that this region is mixture of AA2024-O and AA5083-H112. Based on these observations, it is seen that WNZ with insert AA2024-O material is not completely mixed. Variation in the alloying element distribution may have a consequence on the mechanical properties, especially strength and hardness of the WNZ.

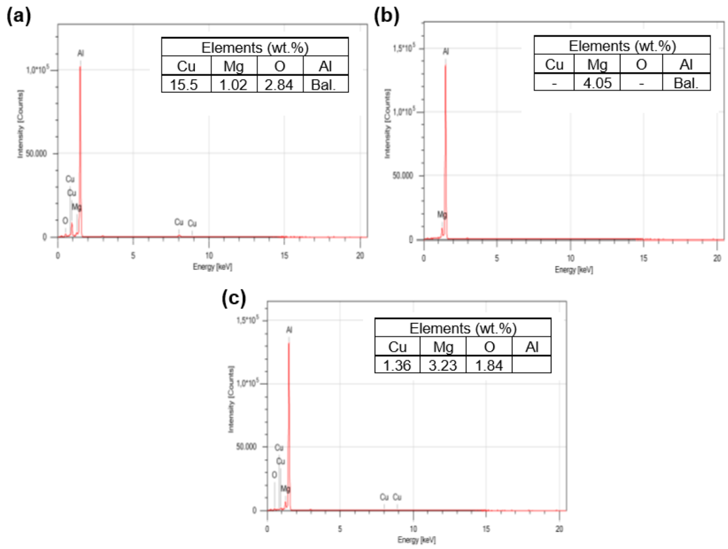

Figure 4. The EDX spectra of WNZ of FSWed AA5083-H112 with inserted AA2024-O taken from regions marked: (a) A, (b) B and (c) C in Fig. 3(a).

Microhardness Distribution

The hardness profiles of FSWed AA5083-H112 joints without and with inserted AA2024-O material are depicted in Figure 6. The average value of hardness for AA5083-H112 is around 80.0 HV. The hardness then decreases steadily across HAZ till the minimum value is achieved at TMAZ. Furthermore, a small increase in the hardness occurs in WNZ. Such a hardness distribution is matched to U-shaped profile. The softening which occurs in HAZ, TMAZ and WNZ is associated with annealing effect and coarsening of the microstructure due to heating during FSW process. This finding is in line with the Hall-Petch equation which states that the yield strength is linearly proportional to $d^{-1/2}$ with d is grain size [25].

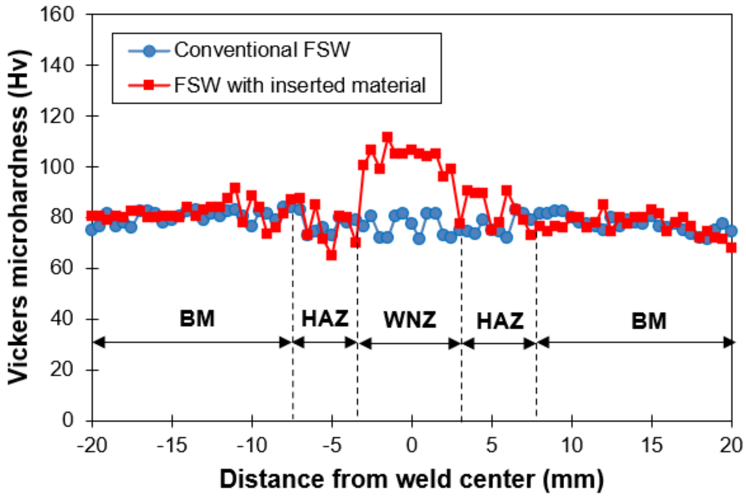

Figure 5. The hardness distribution across the transverse section of FSWed AA5083-H112 joints with and without inserted AA2024-O material

The FSW joint with the addition of insert material shows peak of hardness, typically 112.0 HV in WNZ in contrast to conventional FSW joints. The increased hardness within WNZ is significantly attributed to the reprecipitation hardening due to inserted Al-Cu alloy material as the following: Supersaturated solid solution → GP1 zone → GP2 zone (θ" phase) → θ' → θ (Al_2Cu) [26]. The hardness then begins to decline in TMAZ and HAZ as observed in both AS and RS due to softening as discussed previously.

Tensile Properties

Fig. 6 depicts tensile properties of FSW joints of AA5083-H112 with and without inserted AA2024-O material presented in the forms of ultimate tensile strength (σ_u), yield strength (σ_y) and % ductility. It is seen that the value of σ_u for FSW joint without inserted material is around 220.0 MPa. An improvement in σ_u value of FSW joints is observed with the addition of inserted material with the value of σ_u is around 249.8 MPa. Apart from ultimate tensile strength, the yield strength and ductility of FSW joints of AA5083-H112 increase as the AA2024-O sheet are inserted.

After tensile tests, fracture surfaces of FSW joints with and without inserted material are analyzed using optical microscopy (Figure 7) combined with scanning electron microscopy (SEM) as shown in Figure 8. The location of failure in FSW weld without inserted material in Figure 7(a) is initiated at the bottom of WNZ in AS with the fracture surface is normal to the direction of applied tensile axis. Afterwards, the crack propagates across WNZ at an angle of 45° to the applied tensile axis, suggesting that the static failure is mainly caused by shear stress as normally found in ductile materials. In contrast, the FSW joints with inserted material in Figure 7(b) start to crack at the unmixed region between insert material and base metal at the bottom of the WNZ. The crack then propagates along this region across WNZ in AS.

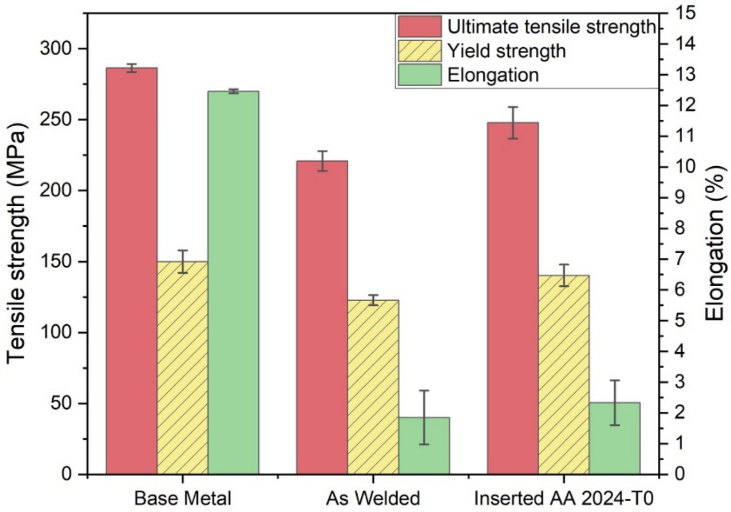

Figure 6. Tensile properties of FSWed AA5083-H112 joints with and without inserted AA2024-O material.

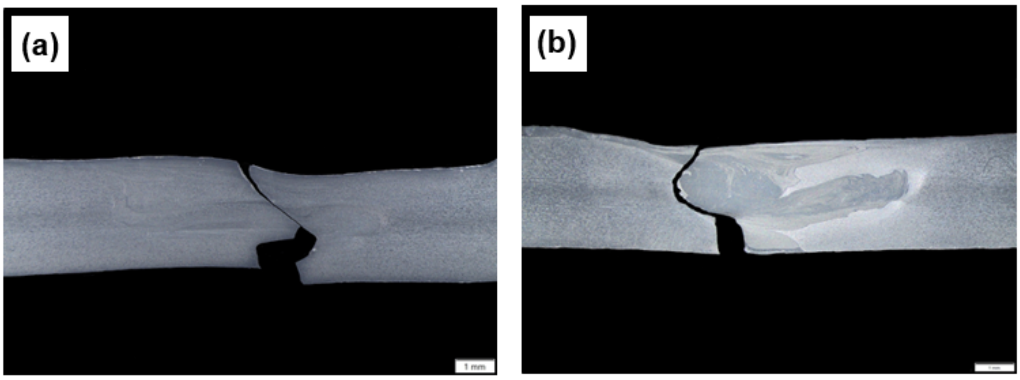

Figure 7. Static fractures of FSWed AA5083-H112 joints: (a) without, and (b) with inserted AA2024-O material

Figure 8 shows SEM fractographic images of the fractured surface of the FSW joints with and without inserted material. Consistent with the result in Figure 8(a), the fracture surface of FSW joint with no insert material shows the presence of dimples indicating a ductile fracture mode. It has been reported that the formation of dimples under tensile stress is associated with voids which usually nucleate at the second phases such inclusions or precipitates. The voids are then coalesced among them making the crack to propagate [27]. Furthermore, the fracture surface observation on the FSW joint with inserted material shows the presence of dimples similar to that found in the conventional FSW joint. Unfortunately, the present investigation fails to find evidence of unmixed region between the inserted material and base metal as indicated in Figure 7(b.) It does not mean that such a region does not exist. It seems that the diffusion between the inserted AA2024-O material and the AA5083-H112 base material is effective in establishing good bonding so that it appears to be homogeneous.

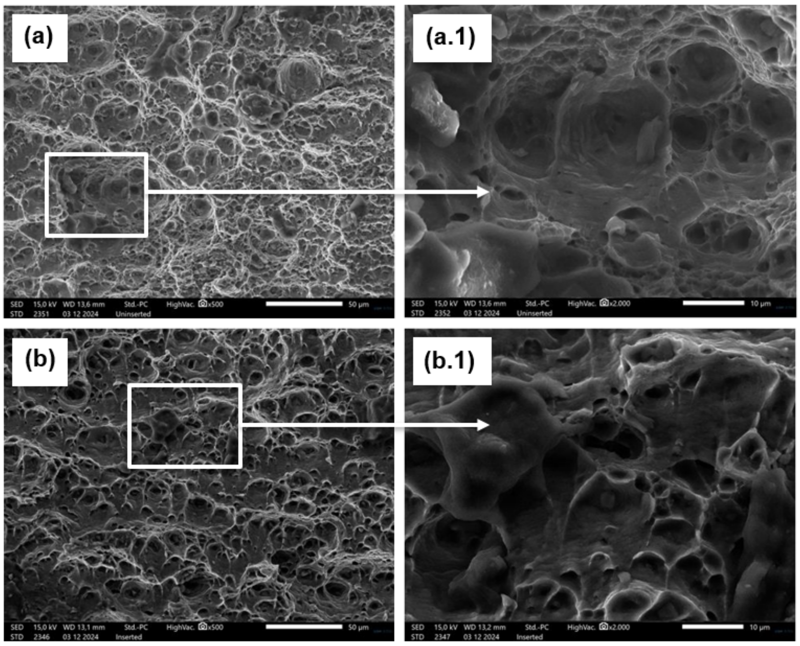

Figure 8. SEM fractographs of FSWed AA5083-H112 joints with and without inserted material after tensile tests

Conclusion

The current research has attempted to investigate the effectiveness of inserted AA2024-O material in improving the quality of FSWed AA5083-H112 joints, and the following conclusions are drawn:

1. The WNZ microstructure of FSW joint under AA2024-O inserted material is marked by the presence of unmixed region between AA2024-O and AA5083-H112 base metal indicating that complete mixing between the two materials is not completely achieved.
2. Inserting heat treatable AA2024-O aluminum in FSW process of the AA5083-H112 plates increases the hardness of WNZ accompanied by reduction in TMAZ hence modifying the hardness profile from U-shaped profile to become W-shaped profile due to re-precipitation during welding.
3. The strength of the FSW joints under inserted material increases from 220.0 MPa to 249.8 MPa owing to re-precipitation during welding. Fractographic study shows that the crack nucleates at the unmixed region in the bottom part of the WNZ. Therefore, this location is the weakest part of inserted FSW joints

Acknowledgments

The authors would like to express their sincere gratitude to the Materials Engineering Laboratory, Department of Mechanical and Industrial Engineering, Universitas Gadjah Mada, for providing the facilities required for this study.

References

[1] M. Abdulstaar, M. Mhaede, M. Wollmann, and L. Wagner, “Investigating the effects of bulk and surface severe plastic deformation on the fatigue, corrosion behaviour and corrosion fatigue of AA5083,” *Surf. Coatings Technol.*, vol. 254, pp. 244–251, 2014, doi: 10.1016/j.surfcoat.2014.06.026.

[2] R. L. Holtz, P. S. Pao, R. A. Bayles, T. M. Longazel, and R. Goswami, “Corrosion-Fatigue Behavior of Aluminum Alloy 5083-H131 Sensitized at 448 K (175 °C),” *Metall. Mater. Trans. A*, vol. 43, no. 8, pp. 2839–2849, Aug. 2012, doi: 10.1007/s11661-011-0866-x.

[3] B. Gungor, E. Kaluc, E. Taban, and A. SIK ŞŞ, “Mechanical and microstructural properties of robotic Cold Metal Transfer (CMT) welded 5083-H111 and 6082-T651 aluminum alloys,” *Mater. Des.*, vol. 54, pp. 207–211, Feb. 2014, doi: 10.1016/j.matdes.2013.08.018.

[4] W. Thomas, E. Nicholas, J. Needham, M. Murch, p Tample-Smith, and C. Dawes, *Friction Stir Butt Welding* . London: UK Patent Office, 1991.

[5] M. Bachmann, J. Carstensen, L. Bergmann, J. F. dos Santos, C. S. Wu, and M. Rethmeier, “Numerical simulation of thermally induced residual stresses in friction stir welding of aluminum alloy 2024-T3 at different welding speeds,” *Int. J. Adv. Manuf. Technol.*, vol. 91, no. 1–4, pp. 1443–1452, Jul. 2017, doi: 10.1007/s00170-016-9793-8.

[6] M. Shunmugasundaram, A. Praveen Kumar, N. K. Amudhavalli, and S. Sivasankar, “Parametric optimization on tensile strength of friction stir butt joints of dissimilar AA6061 and AA5052 aluminium alloys by Taguchi technique,” *Mater. Today Proc.*, vol. 27, pp. 1258–1262, 2020, doi: 10.1016/j.matpr.2020.02.166.

[7] P. S. Kumar and M. S. Chander, “Effect of tool pin geometry on FSW dissimilar aluminum alloys - (AA5083 & AA6061),” *Mater. Today Proc.*, vol. 39, pp. 472–477, 2021, doi: 10.1016/j.matpr.2020.08.204.

[8] N. R. Mandal, *Aluminum Welding 2nd Ed.*, 2nd ed. New Delhi, India: Marisa Publishing House Pvt. Ltd., 2005.

[9] Y. Qiu *et al.*, “Enhanced mechanical property and corrosion resistance of alloy 5182 FSW joints by Sc and Zr alloying,” *Mater. Charact.*, vol. 194, p. 112412, Dec. 2022, doi: 10.1016/j.matchar.2022.112412.

[10] N. Dialami, M. Cervera, M. Chiumenti, and C. Agelet de Saracibar, “A fast and accurate two-stage strategy to evaluate the effect of the pin tool profile on metal flow, torque and forces in friction stir welding,” *Int. J. Mech. Sci.*, vol. 122, pp. 215–227, Mar. 2017, doi: 10.1016/j.ijmecsci.2016.12.016.

[11] M. Prihajatno, M. N. Ilman, R. A. Sriwijaya, M. R. Muslih, and R. Apriansyah, “Tensile and fatigue properties of friction stir AZ31B-H24 magnesium alloy welded joints under the influences of pin geometry and tool rotation rate,” *J. Adv. Join. Process.*, vol. 9, p. 100202, Jun. 2024, doi: 10.1016/j.jajp.2024.100202.

[12] K. J. Quintana and J. L. L. Silveira, “Mechanistic models and experimental analysis for the torque in FSW considering the tool geometry and the process velocities,” *J. Manuf. Process.*, vol. 30, pp. 406–417, Dec. 2017, doi: 10.1016/j.jmapro.2017.09.031.

[13] S. Babu, K. Elangovan, V. Balasubramanian, and M. Balasubramanian, “Optimizing friction stir welding parameters to maximize tensile strength of AA2219 aluminum alloy joints,” *Met. Mater. Int.*, vol. 15, no. 2, pp. 321–330, Apr. 2009, doi: 10.1007/s12540-009-0321-3.

[14] Z. Zhang, B. L. Xiao, and Z. Y. Ma, “Effect of welding parameters on microstructure and mechanical properties of friction stir welded 2219Al-T6 joints,” *J. Mater. Sci.*, vol. 47, no. 9, pp. 4075–4086, May 2012, doi: 10.1007/s10853-012-6261-1.

[15] S. R. Ren, Z. Y. Ma, and L. Q. Chen, “Effect of welding parameters on tensile properties and fracture behavior of friction stir welded Al–Mg–Si alloy,” *Scr. Mater.*, vol. 56, no. 1, pp. 69–72, Jan. 2007, doi: 10.1016/j.scriptamat.2006.08.054.

[16] A. Rodríguez *et al.*, “Burnishing of FSW Aluminum Al–Cu–Li Components,” *Metals (Basel).*, vol. 9, no. 2, p. 260, Feb. 2019, doi: 10.3390/met9020260.

[17] S. Hassanifard, H. Mousavi, and A. Varvani-Farahani, “The influence of low-plasticity burnishing process on the fatigue life of friction-stir-processed Al 7075-T6 samples,” *Fatigue Fract. Eng. Mater. Struct.*, vol. 42, no. 3, pp. 764–772, Mar. 2019, doi: 10.1111/ffe.12950.

[18] M. Bahrami, N. Helmi, K. Dehghani, and M. K. B. Givi, “Exploring the effects of SiC reinforcement incorporation on mechanical properties of friction stir welded 7075 aluminum alloy: Fatigue life, impact energy, tensile strength,” *Mater. Sci. Eng. A*, vol. 595, pp. 173–178, Feb. 2014, doi: 10.1016/j.msea.2013.11.068.

[19] T. Singh, S. K. Tiwari, and D. K. Shukla, “Mechanical and microstructural characterization of friction stir welded AA6061-T6 joints reinforced with nano-sized particles,” *Mater. Charact.*, vol. 159, p.

110047, Jan. 2020, doi: 10.1016/j.matchar.2019.110047.
[20] A. W. A. Lenin, N. Periyasamy, and L. George, "Influence of Interlayer Thickness (Zn) on the Properties of Al 7020 FSW Joints," *Mater. Res.*, vol. 19, no. 4, pp. 817–823, Jun. 2016, doi: 10.1590/1980-5373-MR-2016-0163.
[21] S. G. Shiri, A. Sarani, S. R. E. Hosseini, and G. Roudini, "Diffusion in FSW Joints by Inserting the Metallic Foils," *J. Mater. Sci. Technol.*, vol. 29, no. 11, pp. 1091–1095, Nov. 2013, doi: 10.1016/j.jmst.2013.07.003.
[22] S. Dixit, M. H. C., S. V. Kailas, and K. Chattopadhyay, "Role of insert material on process loads during FSW," *Int. J. Adv. Manuf. Technol.*, vol. 91, no. 9–12, pp. 3427–3435, Aug. 2017, doi: 10.1007/s00170-016-9974-5.
[23] L. Fratini, G. Buffa, D. Palmeri, J. Hua, and R. Shivpuri, "Material Flow in FSW of AA7075-T6 Butt Joints: Continuous Dynamic Recrystallization Phenomena," *J. Eng. Mater. Technol.*, vol. 128, no. 3, pp. 428–435, Feb. 2006, doi: 10.1115/1.2204946.
[24] K. N. Krishnan, "On the formation of onion rings in friction stir welds," *Mater. Sci. Eng. A*, vol. 327, no. 2, pp. 246–251, Apr. 2002, doi: 10.1016/S0921-5093(01)01474-5.
[25] "Mechanical metallurgy - Dieter_ George Ellwood".
[26] D. Sadeghi-Nezhad *et al.*, "The effect of cold rolling, double aging and overaging processes on the tensile property and precipitation of AA2024 alloy," *J. Mater. Res. Technol.*, vol. 9, no. 6, pp. 15475–15485, Nov. 2020, doi: 10.1016/j.jmrt.2020.11.005.
[27] W. D. Callister and J. G. David Rethwisch, "MATERIALS SCIENCE and ENGINEERING."